Revision 1

Chromium-bearing phases in the Earth's mantle: Evidence from experiments in the Mg_2SiO_4–$MgCr_2O_4$ system at 10–24 GPa and 1600 °C

EKATERINA A. SIROTKINA[1,2,3,*], ANDREY V. BOBROV[1,2,3], LUCA BINDI[4,5], TETSUO IRIFUNE[6,7]

[1] Vernadsky Institute of Geochemistry and Analytical Chemistry of Russian Academy of Sciences, Moscow, Russia 119991
[2] Department of Petrology, Geological Faculty, Moscow State University, Moscow, Russia 119991
[3] Institute of Experimental Mineralogy of Russian Academy of Sciences, Chernogolovka, Russia, 142432
[4] Dipartimento di Scienze della Terra, Università di Firenze, Via La Pira 4, 50121 Florence, Italy
[5] CNR - Istituto di Geoscienze e Georisorse, sezione di Firenze, Via La Pira 4, 50121 Florence, Italy
[6] Geodynamics Research Center, Ehime University, Matsuyama 790-8577, Japan
[7] Earth-Life Science Institute, Tokyo Institute of Technology, Tokyo 152-8550, Japan

*Corresponding Author: ekaterina.a.sirotkina@gmail.com

Abbreviations

Ak	akimotoite ($MgSiO_3$ with ilmenite-type structure)
anhB	anhydrous phase B ($(Mg,Cr)_{14}(Si,Cr)_5O_{24}$)
Brd	bridgmanite ($MgSiO_3$ with perovskite-type structure)
Ct	$MgCr_2O_4$ with calcium-titanate structure
Chr	chromite
Esk	eskolaite (Cr_2O_3)
Fo	forsterite
*f*Per	ferropericlase
Grt	garnet
Knr	knorringite ($Mg_3Cr_2Si_3O_{12}$)
Maj	majorite ($Mg_4Si_4O_{12}$)
MChr	magnesiochromite ($MgCr_2O_4$)
mCt	$Mg(Si,Mg)(Cr,Mg)O_4$ with modified calcium titanate-type structure
mLd	$Mg_2Cr_2O_5$ with modified ludwigite-type structure
Ol	olivine
OPx	orthopyroxene
Per	periclase (MgO)
Prp	pyrope ($Mg_3Al_2Si_3O_{12}$)
Rgw	ringwoodite

Wad wadsleyite

ABSTRACT

Phase relations in the system Mg_2SiO_4–$MgCr_2O_4$ were studied at 10–24 GPa and 1600°C using a high-pressure Kawai-type multi-anvil apparatus. We investigated the full range of starting compositions for the forsterite-magnesiochromite system to derive a *P–X* phase diagram and synthesize chromium-bearing phases, such as garnet, wadsleyite, ringwoodite, and bridgmanite of a wide compositional range. Samples synthesized at 10 GPa contain olivine with small chromium content and magnesiochromite. Mg_2SiO_4 wadsleyite is characterized by the pressure-dependent higher chromium solubility (up to 7.4 wt % Cr_2O_3). The maximal solubility of chromium in ringwoodite in the studied system (~18.5 wt% Cr_2O_3) was detected at P = 23 GPa, which is close to the upper boundary of the ringwoodite stability. Addition of chromium to the system moves the boundaries of olivine/wadsleyite and wadsleyite/ringwoodite phase transformations to lower pressures. Our experiments simulate Cr-rich phase assemblages found as inclusions in diamonds, mantle xenoliths, and UHP podiform chromitites.

Keywords: Magnesiochromite, Forsterite, Olivine, Wadsleyite, Ringwoodite, Knorringite, Majorite, Bridgmanite, Mantle, High-*P*-*T* experiments, Phase relations

INTRODUCTION

The Earth's upper mantle consists of olivine (~60 vol %), ortho-, clinopyroxenes, spinel, and garnet (Ringwood 1966; Harte 2010; Pushcharovsky and Pushcharovsky 2012). The phases of the transition zone include wadsleyite/ringwoodite and majoritic garnet. At higher pressures (corresponding to the lower mantle) the ringwoodite-bearing assemblage converts into a bridgmanite + ferropericlase association with a minor amount of $CaSiO_3$ perovskite (Liu 1976;

Ito and Takahashi 1989). Some of these phases are observed as inclusions in natural diamonds (Harte 2010). Mantle minerals show variable concentrations of minor elements. Although the solubility of minor elements in high-pressure phases is poorly studied, it is known that even small concentrations of these elements may significantly influence the physical properties as well as the crystal-chemical peculiarities of mantle phases and control the physicochemical parameters of the main phase equilibria (Panero et al. 2006; Andrault 2007; Sirotkina et al. 2015).

Chromium is one of such elements with the low bulk concentrations in the Earth's mantle (0.42 wt % Cr_2O_3) (Ringwood 1966), although some mantle phases (garnet, chrome spinel, etc.) are characterized by significant Cr contents (Stachel and Harris 1997; Harte et al. 1999). The studies of phase equilibria in multicomponent mantle systems (pyrolite and peridotites) (Hirose 2002; Irifune 1987; Irifune and Ringwood 1987) provide only limited information on interphase partitioning of chromium, which is mostly explained by its very low concentrations in starting compositions.

The highest Cr concentrations have been documented in such mantle phases as chrome spinel (Meyer and Boyd, 1972; Sobolev 1974). Magnesiochromite ($MgCr_2O_4$) is an important end-member of chrome spinel in mantle peridotites (Fig. 1). Its concentration in chrome spinel from inclusions in diamonds and xenoliths of Grt-peridotite reaches 95 and 85 mol % (63–68 wt % and 57–63 wt % Cr_2O_3), respectively (Meyer and Boyd 1972; Sobolev 1974). The lowest chromium content (25–38 wt % Cr_2O_3) is typical of spinel from Sp-peridotite xenoliths in kimberlite and alkali basalt. Chrome spinel from ophiolithes occupies an intermediate position between the Grt- and Sp-peridotite xenoliths. There is a clear positive correlation between chromium content in Cr-spinel from peridotites and both the degree of partial melting and pressure (Dick and Bullen 1984).

Although the concentrations of Cr in $(Mg,Fe)_2SiO_4$ polymorphs and bridgmanite are rather low, abundance of these phases in the mantle allows us to consider them as the major hosts for chromium. Mantle olivine in association with chromite contains an exceptionally high content of chromium (up to 1.10 wt. % Cr_2O_3) (Phillips et al. 2004). More Cr-rich phases (1.49 wt. % Cr_2O_3) with the composition of olivine were identified in UHP podiform chromitites of the Luobusa ophiolite, Southern Tibet (Robinson et al. 2004; Liang et al. 2014); such phases could be originally ringwoodite, then transformed to a Mg-Fe silicate with an octahedral shape.

Gudfinnsson and Wood (1998) studied the effect of minor elements, such as Ni, Cr, Al, and H, on the depth and thickness of olivine-wadsleyite transition. The authors demonstrated that the maximum concentration of Cr_2O_3 that could be dissolved in wadsleyite was ~2.0 wt% at 14 GPa and 1600°C. They suggested that effects of these minor elements on the properties of the 410 km seismic discontinuity (olivine/wadsleyite transition) was negligible.

It should be noted that experiments in this study are unbuffered so both valence states of chromium are possible. It is evident from some experimental studies (Hanson and Jones 1998; Berry and O'Neill 2004; Papike et al. 2004) that Cr^{2+} is quite abundant in melts at high temperature, but may enter olivine under very reduced conditions (IW-1 (Papike et al. 2004)). Such conditions are rare in natural processes and may be typical of central inclusions in deep diamonds (Ryabchikov et al. 1981), lunar basalts, and meteorites. Therefore, we suggest that our study is relevant to most of high-pressure assemblages of the Earth's mantle.

The system $MgO – SiO_2 – Cr_2O_3$ provides a useful simplification for phase equilibria in the Earth's mantle. This system can be used as a basis for description of more complex (multicomponent or natural) systems containing FeO, Al_2O_3, and CaO, which simulate more closely mantle equilibria and may be used in thermobarometry of mantle assemblages. The $MgSiO_3–Cr_2O_3$ section of the $MgO–SiO_2–Cr_2O_3$ system is well studied in a wide pressure and temperature ranges (Irifune et al. 1982; Turkin et al. 1983; Doroshev et al. 1997; Klemme 2004;

Taran et al. 2004; Zou and Irifune 2012; Sirotkina et al. 2015). Incorporation of chromium in mantle phases was also investigated in the simple model (with the garnet and olivine compositions) (Girnis et al. 2003; Klemme et al. 2004; Turkin and Sobolev 2009) and multi-component (peridotite and pyrolite) (Irifune 1987; Kato et al. 1988) systems.

In this paper, we report phase relations in the Mg_2SiO_4–$MgCr_2O_4$ section of the SiO_2 – MgO – Cr_2O_3 system at 10–24 GPa and 1600°C. The synthesized chromium-bearing phases (Mg_2SiO_4 polymorphs, majoritic garnet, bridgmanite, and phases with the calcium titanate-type structure) and their solid solutions were characterized to investigate their structural peculiarities and compositional changes as a function of pressure. Some implications for the mineralogy of the Cr-bearing phases in the deep mantle including mineral assemblages of the high-pressure podiform chromitite from the Luobusa ophiolite (Southern Tibet) are discussed in the light of our new experimental data.

EXPERIMENTAL AND ANALYTICAL PROCEDURES

Powdered mixtures of chemically pure oxides (MgO, Cr_2O_3, and SiO_2) taken in stoichiometric proportions, homogenized at room temperature using ethanol, and then dried in an oven at 100 °C were used as starting materials. The use of fine-grained (<1 μm) oxides helps to enhance chemical reactions in HP–HT runs, as was demonstrated by Zou and Irifune (2012). Five compositions falling between the forsterite Mg_2SiO_4 and magnesiochromite $MgCr_2O_4$ end members were prepared. The experiments were performed at 10–24 GPa and at a fixed temperature of 1600 °C using a 2,000-t Kawai-type multi-anvil high-pressure apparatus at the Geodynamics Research Center, Ehime University. The cell assembly used in the present experiments is described in Sirotkina et al. (2015). Tungsten carbide cubic anvils with 4.0- and 3.0-mm truncation edge length were applied as the second-stage anvils of the high-pressure apparatus. The pressure medium was a semi-sintered (MgO+17 wt % CoO) octahedron of 10.0

and 8.0 mm in edge length. A tubular $LaCrO_3$ heater was inserted into the pressure medium. The starting material was loaded into a capsule of 1.1 mm in height (0.9 mm for 8/3 cell assembly) and 1.2 mm in diameter made of a platinum foil. The capsule was insulated from the heater by a MgO sleeve. The temperature was measured using a $W_{97}Re_3$ – $W_{75}Re_{25}$ thermocouple with a hot junction positioned in the central part of the heater. The temperature measurement accuracy was ±10 °C. Pressure values at room temperature were calibrated against the load (oil pressure) of the press based on the pressure fixed points: Bi I–II transition at 2.55 GPa, Bi III–V transition at 7.7 GPa, and semiconductor–metal transitions of ZnS at 15.5 GPa and GaAs at 18.3 GPa (Irifune et al. 2004; Zou and Irifune 2012). The effect of temperature on pressure was further corrected using the α–β and β–γ phase transitions of Mg_2SiO_4 (Katsura and Ito 1989; Yamada et al. 2004). As a result, run pressure was controlled within ±0.5 GPa (Irifune et al. 1991). The experiments started with pressurization at ambient temperature to the target pressure, and then the charge was heated to 1600 °C. The heating duration of each run was 3–5 h. After the heating, the samples were quenched by switching off the power supply, subsequently depressurized, and recovered at ambient conditions. As there was some temperature gradient within the sample, only the high-temperature portions near the thermocouple junction were examined in the following analyses.

To exclude the version of metastability in the studied system and confirm the attainment of equilibrium, each run sample was divided into several pieces for microprobe analysis and XRD measurements. To analyze composition of the phases, the samples were embedded into epoxy and polished. Compositions of synthesized phases were studied at the Geological Faculty, Moscow State University, by using a Jeol JSM-6480LV electron microscope equipped with an energy-dispersive X-ray detector INCA Energy. The following standards were used: synthetic SiO_2, MgO, and Cr_2O_3 for Si, Mg, and Cr, respectively. Phase compositions in each run were determined from the average of 3–6 analyses performed at 20 kV accelerating voltage, 10 nA

beam current. The samples were homogeneous, without significant differences in textures and mineral composition and without zoning of individual grains, thus confirming that the chemical equilibrium was achieved in the runs. We applied the SkyScan software (CT-An) for precise determination of the bulk concentration of garnet in the sample by using BSE images. Small crystals of chromium-rich phases, including olivine, wadsleyite, ringwoodite, anhydrous phase B and $Mg[(Cr,Mg)(Si,Mg)]O_4$ with distorted calcium titanate-type structure, handpicked under a reflected light microscope from the experimental products, were preliminarily examined at the CRIST Center of the University of Florence, Italy, with a Bruker–Enraf MACH3 single-crystal diffractometer using graphite-monochromatized Mo*K*α radiation. The data collections were then done with an Oxford Diffraction Xcalibur 3 diffractometer (X-ray MoKα radiation, $\lambda = 0.71073$ Å) fitted with a Sapphire 2 CCD detector at the CRIST Center of the University of Florence, Italy. Intensity integration and standard Lorentz-polarization corrections were done with the CrysAlis RED (Oxford Diffraction 2006) software package. The program ABSPACK of the CrysAlis RED package (Oxford Diffraction 2006) was used for the absorption correction.

RESULTS

P–X diagram for the system Mg_2SiO_4–$MgCr_2O_4$ at 1600°C and textural relationships in the run products

At 10–24 GPa and 1600°C we studied the full range of the starting materials in the Mg_2SiO_4 (Fo)–$MgCr_2O_4$ (MChr) system in increments of 20–30 mol % MChr and 1–3 GPa, which allowed us to synthesize chromium-bearing phases with a wide compositional range. The main phases obtained in experiments were olivine (Ol), wadsleyite (Wad), ringwoodite (Rgw), $MgCr_2O_4$ (Ct) and $Mg(Si,Mg)(Cr,Mg)O_4$ with modified calcium titanate-type structure (mCt) (Bindi et al. 2015a), garnet (Grt) of the majorite (Maj)–knorringite (Knr) composition, chromium-bearing bridgmanite (Brd) and periclase (Per), eskolaite (Esk), $Mg_2Cr_2O_5$ with

modified ludwigite-type structure (mLd), $MgCr_2O_4$ with spinel-type structure (MChr), and anhydrous phase B $(Mg,Cr)_{14}(Si,Cr)_5O_{24}$ (anhB) (Bindi et al. 2016). Run conditions and phase compositions of the samples are reported in Table 1. Phase relations in the Mg_2SiO_4–$MgCr_2O_4$ system can be described in terms of the three-component system SiO_2–MgO–Cr_2O_3 (Fig. 2). Textural relationships in experimental samples are evident from BSE photomicrographs (Fig. 3); Figure 4 shows the P–X diagram for the system Mg_2SiO_4–$MgCr_2O_4$ at 1600°C. This diagram illustrates the phase relations, as well as the compositions of associated phases. Such approach was successfully applied in some previous studies (e.g., Sirotkina et al. 2015).

An association of chromium-bearing olivine and magnesiochromite (Ol + MChr) is stable at a pressure of 10 GPa over a wide range of the starting compositions. The texture of the experimental sample shown in Fig. 3a is composed of relatively large olivine crystals with a size of >50 μm and uniformly distributed MChr grains, often interstitial with a size of <30 μm. The fraction of spinel in the sample increases with increasing chromium content in the starting composition from ~27 vol % in run 2632-30 (30 mol % MChr in the starting composition) to 80 vol % in run 2632-80 (80 mol % MChr in the starting composition).

Increase of pressure for Cr-poor bulk compositions (0–8 mol % MChr in the starting composition) results in the formation of a single-phase field of wadsleyite (Fig. 4). At a pressure of > 12 GPa, an association of Grt, mLd, and anhB is stabilized in the range of starting compositions from 8 to 60 mol % MChr by the following reactions (*a* and *b* in Figs. 2a and 2b):

$$8Mg_2SiO_4\,(Ol/Wad/mCt) + MgCr_2O_4\,(MChr/mCt) =$$
$$= Mg_{14}Si_5O_{24}\,(anh\ B) + Mg_3Cr_2Si_3O_{12}\,(Knr) \qquad (a)$$

$$5MgCr_2O_4\,(MChr/mCt) + 3Mg_2SiO_4\,(Ol/Wad/mCt) =$$
$$= Mg_3Cr_2Si_3O_{12}\,(Knr) + 4Mg_2Cr_2O_5\,(mLd) \qquad (b_1)$$

$MgCr_2O_4$ (MChr/mCt) + Mg_2SiO_4 (Ol/Wad/mCt) =

= $MgSiO_3$ (Maj) + $Mg_2Cr_2O_5$ (mLd) (b_2)

As Knr–Maj garnet and anhB plot outside the Fo–MChr section on the SiO_2–MgO–Cr_2O_3 diagram (Fig. 2a), the studied system should be considered as pseudo-binary. Further increase in pressure results in the formation of an association of Wad and mCt (reaction *a* in Fig. 2a proceeds to the left). Wad associated with mCt is represented by relatively large euhedral crystals with a size of <70 µm. mCt forms small subhedral grains (Fig. 3b).

Increase in chromium content in the starting composition (from 35 to 60 mol % MChr) results in the formation of an association of Grt and mCt. Reactions b_1 and b_2 in Fig. 2b illustrate the formation of the Knr and Maj end-members of garnet, respectively. Mass balance in the system requires the formation of mLd as well. The texture of the samples is formed by relatively large crystals of mCt with a size up to 60 µm, smaller elongated mLd grains (<25 µm), and relatively small (<15 µm) euhedral Grt crystals (Fig. 3c).

At a pressure of ~12 GPa, an association of Ol and Ct is replaced by the paragenesis of Grt, Esk, and mLd in the chromium-rich part of the system. The first appearance of an association mLd + Esk is controlled by the reaction (line *c* in Fig. 2b):

$2MgCr_2O_4$ (MChr/Ct) = $Mg_2Cr_2O_5$ (mLd) + Cr_2O_3 (Esk). (*c*)

Appearance of an association Esk + mLd provides additional evidence for the pseudo-binary character of the studied Fo–MChr system.

The formation of Ct in association with Maj-rich Grt (or Cr-bearing Brd) and mLd at a pressure of >18 GPa is controlled by the reaction *d* in Fig. 2c:

$Mg_3Cr_2Si_3O_{12}$ (Knr) + $Mg_2Cr_2O_5$ (mLd) = $2MgCr_2O_4$ (Ct) + $3MgSiO_3$ (Maj/Brd). (*d*)

Ct forms relatively large grains with a size up to 50 μm. With increasing pressure, the field of Ct expands to the lower Cr concentrations in the system due to increasing Mg_2SiO_4 solubility in this phase.

At a pressure of >18 GPa, two garnet-bearing associations (Grt + Wad + mLd (Fig. 3d) and Grt + Ct + mLd) are stable within a wide range of starting compositions (10–90 mol % MChr). The first of them is observed in Samples 2651-50 and 2645-10 at 19 GPa. At a pressure of ~20 GPa, Wad is replaced by ringwoodite (both phases associate with Cr-rich Grt and mLd). The single-phase field of Rgw is typical of the low-chromium starting compositions at ~21 GPa.

The transition from garnet-bearing associations (Grt + Rgw + mLd and Grt + Ct + mLd) to the paragenesis of $MgSiO_3$ bridgmanite (Brd + Rgw + mLd and Brd + Ct + mLd) (Fig. 3e) is observed in a wide range of starting compositions (~15–85 mol % MChr) at *P* >20 GPa. Brd forms small fractured euhedral crystals with a grain size up to 20 μm.

Further increase in pressure (> 23 GPa) results in decomposition of Rgw and formation of an association of Per and Brd (Fig. 3f) for the Cr-poor bulk compositions (0–20 mol % MChr), according to the following reaction (line *e* in Fig. 2c):

Mg_2SiO_4 (Rgw) = $MgSiO_3$ (Brd) + MgO (Per). (*e*)

Cr-bearing Brd and Per are accompanied by mLd for the starting composition with a chromium content from 20 to 45 mol % MChr.

Compositions of the phases

Most phases synthesized in the *system* Mg_2SiO_4–$MgCr_2O_4$ at 10–24 GPa and 1600°C show wide compositional variations. Compositions of the phases produced in our experiments are reported in Table 2.

Olivine and its high-pressure polymorphs (wadsleyite and ringwoodite) in the Mg_2SiO_4–$MgCr_2O_4$ system contain chromium. The maximal solubility of chromium in *olivine* synthesized at 10 GPa reaches ~3.2 wt % Cr_2O_3 (0.060 Cr pfu). Mg_2SiO_4 *wadsleyite* is characterized by the higher chromium solubility increasing with pressure (Fig. 5) up to 7.4 wt % Cr_2O_3 (~0.140 Cr pfu) at 19 GPa. The concentration of chromium in Mg_2SiO_4 *ringwoodite* increases with pressure as well (Fig. 5). The maximal solubility of chromium in Rgw in the Fo–MChr system (~18.5 wt % Cr_2O_3; 0.363 Cr pfu) was detected at a pressure of 23 GPa, which is close to the upper boundary of the Rgw stability.

Spinel (magnesiochromite) associated with Ol has the composition close to $MgCr_2O_4$ with a small silicon admixture (< 1.9 wt % SiO_2, 0.059 Si pfu).

In all runs *$Mg(Mg,Si)(Si,Cr)O_4$ with modified calcium titanate-type structure* (mCt) is characterized by significant amounts of Si (>23 wt % SiO_2, 58–63 mol % Fo) and narrow compositional range. Cr in this phase shows the negative correlation with both Mg and Si (Fig. 6). The concentration of Cr in mCt decreases with increasing pressure, whereas the content of Si and Mg in the octahedral site increases.

$MgCr_2O_4$ with calcium titanate-type structure (Ct) is characterized by a relatively wide compositional range. Mg and Si in this phase are substituted for Cr in the octahedral sites. $MgCr_2O_4$ (Ct) in run products has significant silicon admixture. In the pressure range from 18 to 21 GPa, the concentration of SiO_2 in Ct does not exceed 2.5 wt%. With increasing pressure, the concentration of Si in Ct increases. The maximal solubility of silicon in Ct in the Fo–MChr system (~8 wt % SiO_2; 23 mol % Fo) is observed at a pressure of 24 GPa. However, as is evident from Fig. 6, there is a significant compositional gap between the Ct and mCt phases. $MgCr_2O_4$

(Ct) synthesized in the Maj–Knr system (Sirotkina et al. 2015) contains significantly lower concentrations of silicon in comparison with Ct from the Fo–MChr system (Fig. 6). The dependence of the silicon content on pressure is not evident, since there is no Si in Ct, synthesized at 24 GPa (Bindi et al. 2014a; Sirotkina et al. 2015). This finding is likely explained by association with stishovite at pressures above 20 GPa in the majorite–knorringite system (Sirotkina et al. 2015).

Garnets in all experimental samples have a relatively narrow compositional range and are characterized by a silicon surplus over 3.0 pfu indicating incorporation of the majorite end-member. The concentration of majorite component in garnet increases with pressure that is consistent with the data on the Maj–Knr system (Sirotkina et al. 2015). Thus, the content of Si in the octahedral site is 3.23 pfu (~ 23 mol % Maj in run 2653-80) at 13 GPa, whereas the content of Si in garnet synthesized at 20 GPa is 3.47 pfu (~47 mol % Maj; run 2635-40). Garnets synthesized in the Maj–Knr system with the higher bulk silica concentration are characterized by the higher concentrations of chromium (up to 90 mol % Knr, 30.78 wt % Cr_2O_3) registered at a pressure of 10 GPa (Fig. 7) (Sirotkina et al. 2015).

$Mg_2Cr_2O_5$ with modified ludwigite-type structure (mLd) was synthesized in a wide range of pressure and starting compositions. At relatively low pressures, mLd is characterized by a low Si content, deficiency in Mg, and enrichment in Cr. Mg is substituted for Cr and Si in the mLd structure. It is evident that the composition of this phase depends on pressure: the concentration of Si and Mg increases with pressure, whereas the content of Cr decreases (Table 2). Thus, the maximal solubility of Si in mLd synthesized in the Fo–MChr system (~3.9 wt % SiO_2; 0.15 pfu) was registered at a pressure of 24 GPa (Table 2).

Bridgmanite is characterized by a relatively narrow compositional range (2.8–6.9 wt % Cr_2O_3). The maximal solubility of chromium (~6.9 wt % Cr_2O_3, 0.093 Cr pfu) in Brd was registered at

24 GPa. Cr shows negative correlation with both Mg and Si, which is consistent with a coupled substitution of $Mg^{2+}+Si^{4+}=2Cr^{3+}$.

Periclase synthesized at a pressure of >23 GPa in association with Brd is characterized by a significant amount of silicon (3.8 wt% SiO_2, 0.027 Si pfu) and chromium (22.4 wt% Cr_2O_3, 0.125 pfu Cr). This fact makes Per one of promising Cr concentrators in the Earth's lower mantle.

Anhydrous phase B (anhB) contains the high concentrations of Mg, Si and admixture of Cr matching to the formula $(Mg_{14-x}Cr_x)(Si_{5-x}Cr_x)O_{24}$ ($x \approx 0.30$) (Table 2).

The influence of Cr on cell parameters of mantle phases

As it was mentioned above, all phases with the composition of Mg_2SiO_4 (Ol/Wad/Rgw) synthesized in the Fo–MChr system, contain chromium.

Chromium-bearing olivine with 3.2 wt % Cr_2O_3 (10 GPa, run 2632-30) was found to be orthorhombic, with a space group *Pbnm* and lattice parameters a = 4.752(1), b = 10.195(4), c = 5.979(2) Å, V = 289.68(3) Å^3. Increase in pressure results in the formation of Wad with a higher chromium content (Table 2). As follows from the data on pure Mg_2SiO_4 Wd (Finger et al. 1993), incorporation of chromium in Wad results in a slight decrease in the unit-cell volume. The studied Cr-Wad crystals are orthorhombic with a space group *Imma* and lattice parameters a = 5.690(1), b = 11.456(4), c = 8.250(2) Å, V = 537.81(4) Å^3 (18 GPa, run 2639-10) for the composition $Mg_{1.95}Cr_{0.10}Si_{0.95}O_4$; a = 5.686(2) Å, b = 11.452(6), c = 8.246(4), V = 537.02(1) Å^3 (19 GPa, run 2645-10) for the composition $Mg_{1.93}Cr_{0.14}Si_{0.93}O_4$. Cr-bearing Rgw studied by single crystal X-ray diffraction is characterized by the cubic symmetry with a space group *Fd-3m* and lattice parameters a = 8.063(2), V = 524.23(1) Å^3 (21 GPa, run 2649-10) for the composition $Mg_{1.98}Cr_{0.04}Si_{0.98}O_4$. This value is slightly lower than the a parameter observed for pure Mg_2SiO_4 Rgw (Hazen et al. 1993).

The mechanisms of Cr incorporation in Wad and Rgw are different. The negative correlation between Cr and Si (Fig. 8) with an angular trend line coefficient of –0.5 is observed for Wad. This fact was previously reported in the experimental study by Gudfinnsson and Wood (1998), where the mechanism (1) $2^{VI}Cr^{3+}+^{IV}Mg^{2+}=2^{VI}Mg^{2+}+^{IV}Si^{4+}$ for Cr incorporation in Wad was suggested. Judging from the compositions of Wad obtained in our runs, the same correlation (with an angular coefficient of –0.5) is observed between Mg and Cr (Fig. 8). Hence, we may suggest an alternative mechanism for Cr incorporation in Wad: (2) $^{VI}Cr^{3+}+^{IV}Cr^{3+}=^{VI}Mg^{2+}+^{IV}Si^{4+}$ (Cr substitutes for Mg in the octahedra and for Si in the tetrahedra). Both mechanisms are supported by the negative correlation of Cr with Si and Mg with a slope of –0.5. Thus, we have structures with cation substitutions in both tetrahedral and octahedral sites. In the mechanism (1), Mg replaces Si in the tetrahedral site (inducing an enlargement) and Cr substitutes for Mg in the octahedral sites (inducing a decrease). In the second case (2), there is the similar effect, which is expressed in Cr substitution for both Si in the tetrahedral site (inducing an enlargement) and Mg in the octahedral sites (inducing a decrease). It seems that the lengthening of the T–O bond distances is perfectly counterbalanced by the shortening of the M-O bond distances, thus provoking an almost unchanged unit-cell volume (Fig. 9).

Rgw is characterized by the negative correlation between Cr and Si with an angular coefficient of –0.5 (Fig. 10). Rgw has the spinel-type structure and, therefore, we suggest a different (from that of Wad) mechanism for Cr incorporation in this phase: Mg substitutes for Si in the tetrahedral site, whereas Cr fully enters Mg-octahedra by the following scheme: $2^{VI}Cr^{3+}+^{IV}Mg^{2+}=2^{VI}Mg^{2+}+^{IV}Si^{4+}$. This substitution would be analogous to that observed in spinel $MgAl_2O_4$ with addition of the $MgCr_2O_4$ component. The unit-cell volume of Rgw remains almost unaffected by the Mg-for-Cr and Si-for-Cr substitutions.

IMPLICATIONS

Implication for the high-Cr mantle mineral assemblages

The main chromium-bearing phases in the Earth's upper mantle are chrome spinel and garnet. The chromium-bearing phases of the transition zone include knorringite-majorite garnet. At higher pressures (corresponding to the lower mantle) the main chromium-rich phases are bridgmanite (up to 1.33 wt % Cr_2O_3) (Zedgenizov et al. 2015) and ferropericlase (up to 2.65 wt % Cr_2O_3) (Harte et al. 1999).

Other chromium-bearing phases in the Earth's mantle are ortho- and clinopyroxenes (with up to 1 wt % and 7.3 wt % Cr_2O_3, respectively), high-pressure post-spinel phases ($Mg(Cr,Fe^{3+})_2O_4$, $Ca(Cr,Fe^{3+})_2O_4$) with the calcium titanate- ($CaTi_2O_4$) and calcium ferrite-type structure ($CaFe_2O_4$) (Kaminsky et al. 2015), and eskolaite (Logvinova et al. 2008).

Structure refinements and *P–X* diagrams of Cr-bearing phases are important for understanding of the influence of Cr on the phase equilibria in the Earth's mantle. It was found that, despite its small content in the mantle, Cr exerts a significant effect on spinel to garnet peridotite transition (MacGregor 1970; O'Neill 1981). Doroshev et al. (1997) established the negative slope of the P–T boundary for the reaction Knr = Esk + En, which was later supported by the detailed thermodynamic analysis of Girnis with co-workers (2003).

The stability field of knorringite has been investigated in several studies (Irifune et al. 1982; Turkin et al. 1983; Klemme 2004; Taran et al. 2004; Zou and Irifune 2012). The pressure- and temperature-dependent compositional variations of garnets have been studied on the pyrope–knorringite (Malinovskii and Doroshev 1974; Klemme 2004; Turkin and Sobolev 2009), majorite–knorringite (Zou and Irifune 2012; Sirotkina et al. 2015), and pyrope–majorite–knorringite (Sirotkina et al. 2016) joins. In these systems, Cr-rich garnets are characterized by the wide compositional range (up to 90 mol % Knr in the Maj–Knr system) and stability field (from 3 GPa in Al-bearing systems to 20 GPa). Our new data show that in the olivine-rich

system (Fo–MChr), Cr-Grt is stable in a quite wide pressure range of 12–20 GPa, whereas the compositional range of Grt is narrower (from 50 to 75 mol % Knr), which is explained by appearance of other Cr-rich phases (anh-B and mCt) (Bindi et al. 2016).

The results of our runs show that even low concentrations of Cr may affect significantly on the bridgmanite stability in the Earth's mantle. In contrast to the Brd stability field in Cr-free and Al-bearing systems (Kubo and Akaogi, 2000; Akaogi et al. 2002), Cr-bearing Brd may be formed at least at 20 GPa (Fig. 4). As the chromium concentration in $(Mg,Fe)SiO_3$ "enstatite" (a retrograde phase inheriting an initial Brd chemical composition) in association with ferropericlase, which were identified as the lower mantle inclusions in diamonds (Harte and Harris, 1994; Hutchison 1997; Stachel et al. 2000, 2002; Davies et al. 2004), reaches 1.33 wt % Cr_2O_3 (Zedgenizov et al. 2015), the formation of such diamonds under the lower mantle conditions may be impugned.

Implication to UHP podiform chromitite

The most Cr-rich mantle assemblages include podiform chromitites in ophiolitic complexes, formed through reaction between mantle peridotite and melt with subsequent magma/melt mixing at an uppermost mantle level (Arai and Yurimoto 1994). Some of them (UHP chromitites), however, contain ultrahigh-pressure (UHP) minerals. For example, high-pressure nature of podiform chromitite in the Luobusa ophiolite (Southern Tibet) is discussed in some works on the basis of finds of diamond (Robinson et al. 2004; Yang et al. 2007), coesite (Yang et al. 2007; Yamamoto et al. 2009), stishovite (Yang et al. 2007), and ringwoodite (Robinson et al. 2004). Recently the data on the composition and relationships of Cr-bearing phases were involved for substantiation of high-pressure origin of the Luobusa chromitite in the processes of deep recycling and upwelling mantle flow (Arai 2013).

In addition to Chr, Ol is the most abundant Cr-bearing phase in Luobusa chromitite and contains up to 1.5 wt % Cr_2O_3 (~1.6 mol % $MgCr_2O_4$) (Liang et al. 2014). Such high concentrations of Cr are not typical of mantle olivine, but according to our experimental data (Fig. 4), Ol may accommodate much more chromium (up to 3.2 wt % Cr_2O_3). As is evident from the data of this study the highest concentrations of Cr_2O_3 in Wad and Rgw are 7.4 and 18.5 wt %, respectively. Ishii et al. (2015) studied the simple systems of $MgCr_2O_4$ and $FeCr_2O_4$ and estimated the highest pressure of the formation of Luobusa chromitite. The authors of the cited paper suggest that absence of the phase assemblage $(Mg,Fe)_2Cr_2O_5 + Cr_2O_3$ stable at 12–18 GPa provides evidence for the lower (<12 GPa) pressures of the origin.

Synthesis of the new phase $Mg(Mg,Cr,Si)_2O_4$ with a distorted calcium titanate-type structure (Bindi et al. 2015; this study) in the model system Fo–MChr (Fig. 4) is of crucial importance in discussion of the origin of Luobusa chromitite. This phase is stable in a wide pressure range (12–18 GPa) and covers a wide range of the starting compositions. As is evident from Fig. 2, this phase occupies an intermediate position between Mg_2SiO_4 and $MgCr_2O_4$ having a narrow compositional range (58–63 mol % Fo). The discovery of this phase impugns the conclusion of (Yamamoto et al. 2009) and limits the highest pressure of the Luobusa chromitite formation by the level of ~12 GPa, above which mCt is stable.

Dobrzhinetskaya et al. (1996) reported that Ol from the Alpe Arami Massif, Switzerland contained numerous oriented ilmenite and chromite intergrowths, which were presumably formed due to the decomposition chromium-rich Wad (Yufeng et al. 2008). Such chromium-wadsleyite was formed at a pressure over 10–15 GPa (300-450 km). The formation of exsolution textures of chromium-bearing phases in Ol (Dobrzhinetskaya et al. 1996; Yufeng et al. 2008) and silicates in Chr (Yamamoto et al. 2009) may be explained by the P–X phase diagram of the Fo–MChr pseudobinary system (Fig. 4). An association of low-Cr olivine and low-Si chromite is stable at a pressure of up to 12 GPa. With increasing pressure, we expect

increase in both concentrations of Si in Chr and Cr in olivine. Decompression will result in exsolution of these phases with exsolution of chromium-bearing phases in olivine and silicates in chromite

ACKNOWLEDGEMENTS

We are grateful to Anton Shatskiy for constructive review and Keith Putirka for help and valuable comments. This study was supported by the Russian Foundation for Basic Research (project no. 16-05-00419). E.A. Sirotkina thanks Geodynamics Research Center, Ehime University, Matsuyama, Japan, for support of her visits in 2016.

References

Akaogi, M., Tanaka, A., and Ito, E. (2002) Garnet–ilmenite–perovskite transitions in the system $Mg_4Si_4O_{12}$–$Mg_3Al_2Si_3O_{12}$ at high pressures and high temperatures: phase equilibria, calorimetry and implications for mantle structure. Physics of the Earth and Planetary Interiors, 132, 303–324.

Andrault, D. (2007) Properties of lower-mantle Al-(Mg,Fe)SiO_3 perovskite. Geological Society of America Special Papers, 421, 15–36.

Arai, S. (2013) Conversion of low-pressure chromitites to ultrahigh-pressure chromitites by deep recycling: a good inference. Earth and Planetary Science Letters, 379, 81–87.

Arai, S., and Yurimoto, H. (1994) Podiform chromitites of the Tari-Misaka ultramafic complex, southwestern Japan, as mantle-melt interaction products. Economic Geology, 89, 1279–1288.

Aulbach, S., Griffin, W.L., Pearson, N.J., O'Reilly, S.Y., Kivi, K., and Doyle, B.J. (2004) Mantle formation and evolution, Slave Craton: constraints from HSE abundances and Re–Os isotope systematics of sulfide inclusions in mantle xenocrysts. Chemical geology, 208, 61–88.

Berry, A.J., and O'Neill, H.St.C. (2004) A XANES determination of the oxidation state of chromium in silicate glasses. American Mineralogist, 89, 790–798.

Bindi, L., Sirotkina, E.A., Bobrov, A.V., Nestola, F., and Irifune, T. (2016) Chromium solubility in anhydrous Phase B. Physics and Chemistry of Minerals, 43, 103–110.

Bindi, L., Sirotkina, E.A., Bobrov, A.V., and Irifune, T. (2015) Structural and chemical characterization of Mg[(Cr,Mg)(Si,Mg)]O_4, a new post-spinel phase with six-fold coordinated silicon. American Mineralogist, 100, 1633–1636.

Bindi, L., Sirotkina, E.A., Bobrov, A.V., and Irifune, T. (2014a) X-ray single-crystal structural characterization of $MgCr_2O_4$, a post-spinel phase synthesized at 23 GPa and 1600°C. Journal of Physics and Chemistry of Solids, 75, 638–641.

Davies, R.M., Griffin, W.L., O'Reilly, S.Y., and McCandless, T.E. (2004) Inclusions in diamond from the K14 and K10 kimberlites, Buffalo Hills, Alberta, Canada: diamond growth in a plume. Lithos, 77, 99–111.

Dick, H.J.B., and Bullen, T.B. (1984) Chromian spine1 as a petrogenetic indicator in abyssal and alpine-type peridotites. In Kimberlites II: The mantle and crust-mantle relationships (ed. J. Komprobst), 295–308.

Dobrzhinetskaya, L., Green, H.W., and Wang, S. (1996) Alpe Arami: A peridotite massif from depths of more than 300 kilometers. Science, 271, 1841–1845.

Doroshev, A.M., Brey, G.P., Girnis, A.V., Turkin, A.I., and Kogarko L.N. (1997) Pyrope – knorringite garnets in the Earth's mantle: Experiments in the MgO-Al_2O_3-SiO_2-Cr_2O_3 system. Russian Geology and Geophysics, 38, 559–586.

Finger, L.W., Hazen, R.M., Zhang, J., Ko, J., and Navrotsky, A. (1993) The effect of Fe on the crystal structure of wadsleyite β-$(Mg_{1-x}Fe_x)_2SiO_4$, $0.00 < x < 0.40$. Physics and Chemistry of Minerals, 19, 361–368.

Girnis, A.V., Brey, G.P., Doroshev, A.M., Turkin, A.I., and Simon, N. (2003) The system MgO-Al_2O_3-SiO_2-Cr_2O_3 revisited: reanalysis of Doroshev et al.'s (1997) experiments and new experiments. European Journal of Mineralogy,15, 953–964.

Gregoire, M., Bell, D.R., and Le Roex, A.P. (2006) Garnet lherzolithes from the Kaapraval Craton (South Africa): Trace element evidence for a metasomatic history. Journal of Petrology, 44, 629–657.

Gudfinnsson, G.H., and Wood, B.J. (1998) The effect of trace elements on the olivine–wadsleyite transformation. American Mineralogist, 83, 1037–1044.

Hanson, B., and Jones, J.H. (1998) The systematics of Cr^{3+} and Cr^{2+} partitioning between olivine and liquid in the presence of spinel. American Mineralogist, 83, 669–684.

Harte, B., and Harris, J.W. (1994) Lower mantle mineral association preserved in diamonds. Mineralogical Magazine, 58, 384–385.

Harte, B., Harris, J.W., Hutchison, M.T., Watt, G.R., and Wilding, M.C. (1999) Lower mantle mineral associations in diamonds from Sao Luiz, Brazil. Mantle Petrology: Field Observations and High Pressure Experimentation: A tribute to Francis R. (Joe) Boyd (The Geochemical Society, Houston), 125–153.

Harte, B. (2010) Diamond formation in the deep mantle: the record of mineral inclusions and their distribution in relation to mantle dehydration zones. Mineralogical Magazine, 74, 189–215.

Hazen, R.M., Downs, R.T., and Finger, L.W. (1993) Crystal chemistry of ferromagnesian silicate spinels:Evidence for Mg-Si disorder. American Minerlaogist, 78, 1320–1323.

Hirose, K. (2002) Phase transitions in pyrolitic mantle around 670-km depth: Implications for upwelling of plumes from the lower mantle. Journal of Geophysical research, 107, 10.1029/2001JB000597.

Hutchison, M.T. (1997) Constitution of the deep transition zone and lower mantle shown by diamonds and their inclusions. Ph.D. thesis, University of Edinburgh, UK.

Irifune, T. (1987) An experimental investigation of the pyroxene–garnet transformation in a pyrolite composition and its bearing on the constitution of the mantle. Physics of the Earth and Planetary Interiors, 45, 324–336.

Irifune, T., Fujino, K., and Ohtani, E. (1991) A new high- pressure form of $MgAl_2O_4$. Nature, 349, 409–411.

Irifune, T., Kurio, A., Sakamoto, S., Inoue, T., Sumiya, H., and Funakoshi, K. (2004) Formation of pure polycrystalline diamond by direct conversion of graphite at high pressure and high temperature. Physics of the Earth and Planetary Interiors, 143, 593–600.

Irifune, T., Ohtani, E., and Kumazawa, M. (1982) Stability field of knorringite $Mg_3Cr_2Si_3O_{12}$ at high pressure and its implication to the occurrence of Cr-rich pyrope in the upper mantle. Physics of the Earth and Planetary Interiors, 27, 263–272.

Irifune, T., and Ringwood, A.E. (1987) Phase transformations in a harzburgite composition to 26 GPa: implications for dynamical behaviour of the subducting slab. Earth and Planetary Science Letters, 86, 365–376.

Ishii, T., Kojitani, H., Fujino, K., Yusa, H., Mori, D., Inaguma, Y., Matsushita, Y., Yamamura, K., and Akaogi, M. (2015) High-pressure high-temperature transitions in $MgCr_2O_4$ and crystal structures of new $Mg_2Cr_2O_5$ and post-spinel $MgCr_2O_4$ phases with implications for ultra-high pressure chromitites in ophiolites. American Mineralogist, 100, 59–65.

Ito, E., and Takahashi, E. (1989) Postspinel transformations in the system Mg_2SiO_4-Fe_2SiO_4 and some geophysical implications. Journal of Geophysical Research, 94(B8), 10637–10646.

Kaminsky, F.V., Wirth, R., and Schreiber, A. (2015) A microinclusion of lower-mantle rock and other minerals and nitrogen lower-mantle inclusions in a diamond. Canadian Mineralogist, 53, 83–104.

Kato, T., Ringwood, A.E., and Irifune, T. (1988) Experimental determination of element partitioning between silicate perovskites, garnets and liquids: constraints on early differentiation of the mantle. Earth and Planetary Science Letters, 89, 123–145.

Katsura, T., and Ito, E. (1989) The system Mg_2SiO_4–Fe_2SiO_4 at high pressure and temperatures: precise determination of stabilities of olivine, modified spinel and spinel. Journal of Geophysical Research, 94, 15663–15670.

Klemme, S. (2004) The influence of Cr on the garnet–spinel transition in the Earth's mantle: experiments in the system $MgO–Cr_2O_3–SiO_2$ and thermodynamic modeling. Lithos, 77, 639–646.

Kubo, A., and Akaogi, M. (2000) Post-garnet transitions in the system $Mg_4Si_4O_{12}$–$Mg_3Al_2Si_3O_{12}$ up to 28 GPa: phase relations of garnet, ilmenite and perovskite. Physics of the Earth and Planetary Interiors, 121, 85–102.

Liang, F., Yang, J., Xu, Z., and Zhao, J. (2014) Moissanite and chromium-rich olivine in the Luobusa mantle peridotite and chromitite, Tibet: Deep mantle origin implication. Journal of Himalayan Earth Sciences (Special Volume), 103.

Liu, L. (1976a) Orthorhombic perovskite phases observed in olivine, pyroxene and garnet at high pressures and temperatures. Physics of the Earth and Planetary Interiors, 11, 289–298.

Liu, L. (1976b) The high-pressure phases of $MgSiO_3$. Earth and Planetary Science Letters, 31, 200–208.

Logvinova, A., Wirth, R., Sobolev, N.V., Seryotkin, Y.V., Yefimova, E.S., Floss, C., and Taylor, L.A. (2008) Eskolaite associated with diamond from the Udachnaya kimberlite pipe, Yakutia, Russia. American Mineralogist, 93, 685–690.

MacGregor, I.D. (1970) The effect of CaO, Cr_2O_3, Fe_2O_3 and Al_2O_3 on the stability of spinel and garnet peridotites. Physics of the Earth and Planetary Interiors, 3, 372–377.

Malinovskii, I.Yu., Doroshev, A.M., and Ran, E.N. (1975) The stability of chro- mium-bearing garnets pyrope: knorringite series. Experimental studies on the mineralogy (1974–1976). Institute of Geology and Geophysics of the Siberian Branch of AS USSR. Novosibirsk, 110–115.

Menzies, A., Westerlund, K., Grütter, H., Gurney, J., Carlson, J., Fung, A., and Nowicki, T. (2004) Peridotitic mantle xenoliths from kimberlites on the Ekati Diamond Mine

property, NWT, Canada: major element compositions and implications for the lithosphere beneath the central Slave craton. Lithos, 77, 395–412.

Meyer, H.O.A., and Boyd, F.R. (1972) Composition and origin of crystalline inclusions in natural diamonds. Geochimica et Cosmochimica Acta, 59, 110–119.

O'Neill, H.S.C. (1981) The transition between spinel lherzolite and garnet lherzolite, and its use as a geobarometer. Contributions to Mineralogy and petrology, 77, 185–194.

Oxford Diffraction (2006) *Crysalis* RED (Version 1.171.31.2) and ABSPACK in CrysAlis RED. Oxford diffraction Ltd. Abingdon. Oxfordshire. England.

Panero, W.R., Akber-Knutson, S., and Stixrude, L. (2006) Al_2O_3 incorporation in $MgSiO_3$ perovskite and ilmenite. Earth and Planetary Science Letters, 252, 152–161.

Papike, J.J., Karner, J.M., and Shearer, C.K. (2004) Comparative planetary mineralogy: V/(Cr+Al) systematics in chromite as an indicator of relative oxygen fugacity. American Mineralogist. 89, 1557–1560.

Phillips, D., Harris, J.W., and Viljoen, K.S. (2004) Mineral chemistry and thermobarometry of inclusions from De Beers Pool diamonds, Kimberley, South Africa. Lithos, 77, 155–179.

Pushcharovsky, D.Yu., and Pushcharovsky, Yu.M. (2012) The mineralogy and the origin of deep geospheres: A review. Earth Science Reviews, 113, 94–109.

Ringwood, A.E. (1977) Synthesis of pyrope-knorringite solid solution series. Earth and Planetary Science Letters, 36, 443–448.

Ringwood, A.E. (1966) The chemical composition and origin of the Earth. In: Advances in Earth science. Hurley, P.M. (Editors), M.I.T. Press, Cambridge. 287–356.

Robinson, P.T., Bai, W.-J., Malpas, J., Yang, J.-S., Zhou, M.-F., Fang, Q.-S., Hu, X.-F., Cameron, S., and Standigel, H. (2004) Ultra-high pressure minerals in the Luobusa Ophiolite, Tibet, and their tectonic implications. In: Malpas, J., Fletcher, C.J.N., Ali, J.R.,

Aitchison, J.C. (Eds.), Aspects of the Tectonic Evolution of China. Geological Society of London, 247–271.

Ryabchikov, I.D., Green, D.H., Wall, V.J., and Brey, G.P. (1981) The oxidation state of carbon in the reduced-velocity zone. Geochemistry International, 18, 148–158.

Sirotkina, E.A., Bobrov, A.V., Bindi, L., and Irifune, T. (2015) Phase relations and formation of chromium-rich phases in the system $Mg_4Si_4O_{12}$–$Mg_3Cr_2Si_3O_{12}$ at 10–24 GPa and 1,600 °C. Contributions to Mineralogy and Petrology, 169:2, DOI: 10.1007/s00410-014-1097-0.

Sobolev, N.V. (1974) Deep-seated inclusions in kimberlites and the problem of upper mantle composition. In: Brown DA, Boyd FR (eds) English translation. American Geophysics Union, Washington, 279.

Stachel, T., and Harris, J.W. (1997) Diamond precipitation and mantle metasomatism-evidence from the trace element chemistry of silicate inclusions in diamonds from Akwatia, Ghana. Contributions to Mineralogy and Petrology, 129, 143–154.

Stachel, T., Harris, J.W., Brey, G.P., and Joswig, W. (2000) Kankan diamonds (Guinea) II: lower mantle inclusion parageneses. Contributions to Mineralogy and Petrology, 140, 16–27.

Stachel, T., Harris, J.W., Aulbach, S., and Deines, P. (2002) Kankan diamonds (Guinea) III: $\delta^{13}C$ and nitrogen characteristics of deep diamonds. Contributions to Mineralogy and Petrology, 142, 465–475.

Taran, M.N., Langer, K., Abs-Wurmbach, I., Frost, D.J., and Platonov A.N. (2004) Local relaxation around $[6]Cr^{3+}$ in synthetic pyrope– knorringite garnets, $[8]Mg_3[6](Al_{1-x}Cr_x^{3+})_2[4]Si_3O_{12}$, from electronic absorption spectra. Physics and Chemistry of Minerals, 31, 650–657.

Turkin, A.I., and Sobolev, N.V. (2009) Pyrope–knorringite garnets: overview of experimental data and natural parageneses. Russian Geology and Geophysics, 50, 1169–1182.

Turkin, A.I., Doroshev, A.M., and Malinovsky, I.Y. (1983) High-pressure and high-temperature investigation of the phases from garnet- bearing associations in the system $MgO–Al_2O_3–Cr_2O_3–SiO_2$. In: "Silicate systems under high pressures", Institute of Geology and Geophysics, Novosibirsk, 5–24 (in Russian).

Yamada, A., Inoue, T., and Irifune, T. (2004) Melting of enstatite from 13 to 18 GPa under hydrous conditions. Physics of the Earth and Planetary Interiors, 147, 45–56.

Yamamoto, S., Komiya, T., Hirose, K., and Maruyama, S. (2009) Coesite and clinopyroxene exsolution lamellae in chromites: In-situ ultrahigh-pressure evidence from podiform chromitites in the Luobusa ophiolite, southern Tibet. Lithos, 109, 314–322.

Yang, J.-S., Dobrzhinetskaya, L., Bai, W.-J., Fang, Q.-S., Robinson, P.T., Zhang, J., and Green, H.W. (2007) Diamond- and coesite-bearing chromitites from the Luobusa ophiolite, Tibet. Geology, 35, 875–878.

Yufeng, R., Fangyuan, C., Jingsui, Y., and Yuanhong, G. (2008) Exsolutions of diopside and magnetite in olivine from mantle dunite, Luobusa ophiolite, Tibet, China. Acta Geologica Sinica (English Edition), 82, 377–384.

Zhou, M.F., Robinson, P.T., Malpas, J., and Li, Z. (1996) Podiform chromitites from the Luobusa ophiolite (Southern Tibet): implications for melt/rock interaction and chromite segregationin the upper mantle. Journal of Petrology, 37, 3–21.

Zou, Y., and Irifune, T. (2012) Phase relations in $Mg_3Cr_2Si_3O_{12}$ and formation of majoritic knorringite garnet at high pressure and high temperature. Journal of Mineralogical and Petrological Sciences, 107, 197–205.

Table 1 Run conditions and products of experiments in the join Mg_2SiO_4-$MgCr_2O_4$

P (GPa)	Run number	N^{system}_{MChr}	Time (hours)	Run products
10	2632-80	80	4	Ol+MChr
	2632-30	30	4	Ol+MChr
12	2627-40	40	3.5	anhB+mLd*+Grt
	2627-10	10	3.5	anhB*+mLd+Grt
13	2653-80	80	5	Grt+mLd+Esk
	2653-30	30	5	Wad+mCt
14	2646-50	50	4	mCt+mLd+Grt
	2646-10	10	4	Wad+mCt
16	2629-80	80	5	Grt+mLd+Esk
	2629-40	40	5	mCt+mLd+Grt
18	2639-30	30	5	Wad+Ct
	2639-10	10	5	Wad+Ct
19	2651-80	80	5	Grt+Ct+mLd*
	2651-50	50	5	Wad+Grt+mLd
	2645-10	10	4	Wad+Grt+mLd*
20	2635-80	80	4	Grt+Ct+mLd
	2635-40	40	4	Rgw+Grt+mLd
21	2634-40	40	5	Rgw+Brd+mLd
	2649-30	30	5	Rgw+Brd+mLd*
	2649-10	10	4	Rgw (with minor Ct*)
23	2647-80	80	4	Brd+Ct+mLd
	2647-30	30	4	Rgw+Brd+mLd*
24	2631-50	50	5	Brd+Ct+mLd
	2631-10	10	5	Brd+Per

Note. * Because of the small grain sizes, compositions of the phases were not analyzed

Table 2 Mean composition of phases produced in the join $MgSiO_3$-$Mg_3Cr_2Si_3O_{12}$ at 10-24 GPa and 1600°C

P, GPa	10				12		13		
Run no.	2632-80		2632-30		2627-40		2653-80		
Phase	Ol	MChr	Ol	MChr	anhB*	Grt	Grt	mLd	Esk
Number of points	5	4	7	4	1	4	5	3	6
MgO	58.19(0.85)	22.14(0.69)	55.14(0.95)	21.94(0.39)	62.6	29.65 (0.22)	29.89 (0.25)	33.31 (0.73)	0.41 (0.08)
SiO_2	40.97(0.57)	1.64(0.40)	41.2(0.47)	1.85(0.19)	32.1	43.59 (0.34)	43.87 (0.57)	0.52 (0.03)	
Cr_2O_3	2.5 (0.46)	74.27(0.43)	3.21(0.57)	74.62(0.70)	5.37	26.38 (0.37)	25.98 (0.85)	65.17 (0.86)	98.63 (0.18)
Total	101.66	98.05	99.55	98.41	100.07	99.62	99.74	99.00	99.04
Formula units per given O									
O	4	4	4	4	24	12	12	5	3
Mg	2.021	1.061	1.952	1.047	13.662	3.259	3.277	1.939	0.016
Si	0.955	0.053	0.979	0.059	4.703	3.217	3.228	0.020	0.000
Cr	0.046	1.889	0.060	1.890	0.622	1.538	1.511	2.013	1.990
Total	3.022	3.003	2.991	2.996	18.986	8.014	8.016	3.973	2.005

P, GPa	12		13		14				
Run no.	2627-10		2653-30		2646-10		2646-50		
Phase	mLd	Grt	Wad	mCt	Wad	mCt	Grt	mLd	mCt
Number of points	4	5	4	3	4	3	4	3	3
MgO	33.87 (0.21)	29.77 (0.54)	54.28 (0.41)	39.62 (0.16)	53.75 (0.46)	40.57 (0.61)	29.96 (0.35)	32.96(0.13)	40.16 (0.57)
SiO_2	0.45 (0.09)	43.91 (0.61)	39.18 (0.96)	21.22 (0.17)	39.39 (0.12)	22.51 (0.20)	44.85 (0.59)	0.74(0.04)	21.81 (0.54)
Cr_2O_3	65.59 (0.58)	26.51 (0.33)	6.31 (0.08)	39.7 (0.18)	6.1 (0.08)	38.69 (0.51)	24.91 (0.21)	63.68(0.4)	38.33 (0.60)
Total	99.91	100.19	99.77	100.54	99.24	101.77	99.72	97.38	100.30
Formula units per given O									
O	5	12	4	4	4	4	12	5	4
Mg	1.954	3.253	1.940	1.589	1.928	1.597	3.268	1.947	1.607
Si	0.017	3.221	0.940	0.572	0.949	0.595	3.285	0.029	0.586
Cr	2.008	1.537	0.120	0.845	0.116	0.808	1.442	1.996	0.814
Total	3.979	8.011	3.000	3.006	2.993	3.001	7.995	3.973	3.007

Table 2 (Contd.)

P, GPa	16			18				19	
Run no.	2629-80			2639-30		2639-10		2651-80	
Phase	Grt	mLd	Esk	Wad	mCt	Wad	mCt	Grt	Ct
Number of points	4	1	3	4	1	5	3	3	3
MgO	29.97 (0.71)	34.28	0.77 (0.58)	54.86 (0.57)	41.25	54.7 (0.88)	40.76 (0.49)	30.78 (0.73)	22.52 (0.16)
SiO_2	44.74 (0.52)	0.92	0.43 (0.87)	40.57 (0.64)	23.23	39.71 (0.56)	22.92 (0.47)	46.17 (0.56)	1.82 (0.05)
Cr_2O_3	24.68 (0.83)	65.27	98.33 (0.93)	4.78 (0.11)	35.85	5.29 (0.05)	34.94 (0.57)	21.41 (0.61)	75.35 (0.53)
Total	99.39	100.47	99.54	100.21	100.33	99.70	98.62	98.36	99.69
Formula units per given O									
O	12	5	3	4	4	4	4	12	4
Mg	3.279	1.960	0.029	1.940	1.634	1.950	1.641	3.364	1.061
Si	3.286	0.035	0.011	0.963	0.618	0.950	0.620	3.387	0.058
Cr	1.433	1.980	1.966	0.090	0.754	0.100	0.746	1.241	1.883
Total	7.998	3.975	2.006	2.992	3.005	3.000	3.007	7.992	3.001

P, GPa	16			19			20		
Run no.	2629-40			2651-50			2635-80		
Phase	Grt	mLd	mCt*	Wad	Grt	mLd	Grt	Ct	mLd
Number of points	4	3	5	3	3	4	4	3	4
MgO	29.92 (0.92)	33.95 (0.25)	40.06 (0.39)	53.29 (0.37)	32.81 (0.23)	34.87 (0.10)	33.36 (0.34)	23.87 (0.23)	34.55 (0.87)
SiO_2	44.69 (0.38)	0.81 (0.20)	22.43(0.18)	40.11 (0.54)	48.5 (0.30)	0.92 (0.05)	49.24 (0.23)	2.39 (0.11)	1.23 (0.09)
Cr_2O_3	24.72 (0.52)	64.25 (0.21)	37.27(0.27)	7.29 (0.84)	19.59 (0.12)	65.25 (0.45)	18.29 (0.19)	74.71 (0.30)	63.36 (0.56)
Total	99.33	99.01	99.76	100.69	100.90	101.04	100.89	100.98	98.59
Formula units per given O									
O	12	5	4	4	12	5	12	4	5
Mg	3.276	1.970	1.606	1.887	3.468	1.980	3.511	1.103	1.994
Si	3.285	0.032	0.603	0.954	3.442	0.035	3.479	0.074	0.048
Cr	1.436	1.978	0.792	0.137	1.099	1.966	1.021	1.832	1.940
Total	7.997	3.979	3.001	2.978	8.009	3.982	8.011	3.010	3.982

Table 2 (Contd.)

P, GPa	19		20			21		23	
Run no.	2645-10		2635-40			2649-30		2647-30	
Phase	Wad	Grt	Rgw	Grt	mLd	Rgw	Brd	Rgw	Brd
Number of points	3	3	5	7	6	4	2	5	3
MgO	53.81 (0.11)	32.11 (0.17)	52.12 (0.85)	32.28 (0.85)	34.85 (0.46)	51.04 (0.26)	39.99 (0.68)	49.85 (0.35)	38.31 (0.38)
SiO_2	38.65 (0.72)	47.34(0.61)	35.88 (0.27)	47.92 (0.24)	1.21 (0.07)	33.86 (0.35)	59.15 (0.10)	32.89 (0.28)	57.14 (0.91)
Cr_2O_3	7.36 (0.19)	20.65 (0.21)	11.87 (0.18)	18.41 (0.77)	64.12(0.18)	15.26 (0.12)	2.82 (0.13)	18.54 (0.5)	4.81 (0.12)
Total	99.82	100.10	99.87	98.61	100.18	100.16	101.96	101.28	100.26
Formula units per given O									
O	4	12	4	12	5	4	3	4	3
Mg	1.929	3.437	1.900	3.481	1.991	1.857	0.986	1.851	0.967
Si	0.930	3.402	0.878	3.469	0.046	0.849	0.979	0.802	0.968
Cr	0.140	1.173	0.230	1.053	1.944	0.297	0.037	0.363	0.064
Total	3.000	8.012	3.007	8.004	3.982	3.003	2.002	3.016	2.000

P, GPa	21				23			24	
Run no.	2634-40			2649-10	2647-80			2631-10	
Phase	Rgw	Brd	mLd	Rgw	Brd	Ct	mLd	Brd	Per
Number of points	1	3	4	1	3	5	3	1	5
MgO	50.89	39.02 (0.58)	34.66 (0.64)	56.35	39.33 (0.41)	23.87 (0.47)	34.69 (0.14)	39.49	71.99 (0.60)
SiO_2	32.98	58.33 (0.40)	2.04 (0.06)	41.58	58.92 (0.55)	3.22 (0.10)	2.13 (0.08)	54.08	3.77 (0.30)
Cr_2O_3	17.07	3.42 (0.42)	62.36 (0.59)	2.15	3.71 (0.08)	72.08 (0.55)	62.08 (0.53)	6.77	22.37 (0.12)
Total	100.94	100.77	99.06	100.08	101.96	99.77	98.90	100.34	98.13
Formula units per given O									
O	4	3	5	4	3	4	5	3	1
Mg	1.872	0.975	1.991	1.979	0.972	1.116	1.995	1.008	0.759
Si	0.814	0.978	0.079	0.980	0.978	0.101	0.082	0.927	0.027
Cr	0.333	0.045	1.901	0.040	0.049	1.788	1.894	0.092	0.125
Total	3.019	1.999	3.971	3.000	1.998	3.005	3.971	2.027	0.911

Table 2 (Contd.)

P, GPa	24		
Run no.	2631-50		
Phase	Brd	Ct	mLd
Number of points	4	3	3
MgO	37.48 (0.23)	29.98 (0.33)	37.86 (0.06)
SiO_2	55.63 (0.43)	7.9 (0.17)	3.94 (0.01)
Cr_2O_3	6.85 (0.83)	62.38 (0.16)	55.67 (0.04)
Total	99.96	100.26	97.47
Formula units per given O			
O	3	4	5
Mg	0.956	1.329	2.165
Si	0.953	0.235	0.151
Cr	0.093	1.467	1.689
Total	2.001	3.031	4.004

Note. * Crystals studied by X-ray diffraction.

FIGURE CAPTIONS

Fig. 1. Composition of chrome spinels from inclusions in diamonds (Davies et al. 2004; Pokhilenko et al. 2004; Deines and Harris 2004), xenoliths in kimberlites and ophiolites (Menzies et al. 2004; Aulbach et al. 2004; Gregoire et al. 2005; Zhou et al. 1996, and references therein).

Fig. 2 Relative position of phases and the studied Mg_2SiO_4 – $MgCr_2O_4$ system within the triangle SiO_2–MgO–Cr_2O_3. Numbers (1–4, 9–11) indicate the maximum of $MgCr_2O_4/Cr_2O_3$ concentrations in olivine (1), wadsleyite (2), Knr-Maj garnet (3), Mg(Mg,Cr)(Si,Cr)O_4 with distorted calcium titanate-type structure (4), ringwoodite (9), bridgmanite (10), anhydrous phase B (11). Numbers (5–8) indicate the maximum of Mg_2SiO_4 concentrations in $Mg_2Cr_2O_5$ with mogified ludwigite-type structure (5), $MgCr_2O_4$ with calcium titanate-type structure (6), magnesiochromite (7), escolaite (8). (12) corresponds to the maximum of SiO_2 and Cr_2O_3 in periclase. Letters in circles (a–e) correspond to the sequence of chemical reactions with increasing pressure and chromium content.

Fig. 3 BSE images of textural relationships in some run products in the system Mg_2SiO_4–$MgCr_2O_4$ at 10–24 GPa and 1600 °C. *a* – Aggregate of olivine and uniformly distributed spinel grains. *b* – Association of wadsleyite and Mg(Mg,Cr)(Si,Cr)O_4 with distorted calcium titanate-type structure. *c* – relatively large crystals of mCt, smaller elongated mLd grains and relatively small euhedral garnet crystals. *d* – Aggregate of Knr-Maj garnet, wadsleyite and $Mg_2Cr_2O_5$ with modified ludwigite-type structure. *e* –Aggregate of $MgSiO_3$ bridgmanite, $MgCr_2O_4$ with a calcium titanate-type structure, and $Mg_2Cr_2O_5$ with modified ludwigite-type structure. *f* – Aggregate of bridgmanite grains with a dense system of fractures and periclase.

Fig. 4. P–X subsection Mg_2SiO_4–$MgCr_2O_4$ of the SiO_2–MgO–Cr_2O_3 phase diagram (Fig. 2). Small open circles denote the composition ("MChr", mol %) of the phases.

Fig. 5. Influence of pressure on Cr concentrations in wadsleyite and ringwoodite synthesized at 13–23 GPa in Mg_2SiO_4–$MgCr_2O_4$ system.

Fig. 6. Variations of Si, Mg, and Cr concentrations in Ct and mCt synthesized in the system Mg_2SiO_4–$MgCr_2O_4$ in comparison with Ct synthesized in the system $Mg_4Si_4O_{12}$–$Mg_3Cr_2Si_3O_{12}$

Fig. 7. Variations of Si, Mg, and Cr concentrations in garnet synthesized at 13–20 GPa and 1600°C in the system Mg_2SiO_4–$MgCr_2O_4$ in comparison with garnet synthesized in the system $Mg_4Si_4O_{12}$–$Mg_3Cr_2Si_3O_{12}$

Fig. 8. Correlation between Cr and Si (*a*) and Cr and Mg (*b*) in wadsleyite synthesized in the system Mg_2SiO_4–$MgCr_2O_4$ at 12–19 GPa and 1600°C.

Fig. 9. Influence of Cr on cell volumes of wadsleyite and ringwoodite. The data for Mg_2SiO_4 Wad/Rgw are taken from (Finger et al. 1993; Hazen et al. 1993).

Fig. 10. Correlation between Cr and Si in ringwoodite synthesized in the system Mg_2SiO_4–$MgCr_2O_4$ at 20–23 GPa and 1600°C.

Figure 1

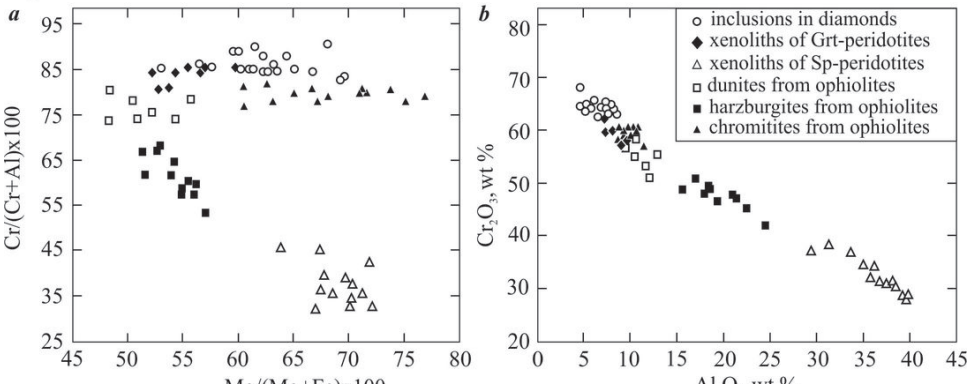
a
Cr/(Cr+Al)x100
Mg/(Mg+Fe)x100
b
Cr_2O_3, wt %
Al_2O_3, wt %
inclusions in diamonds
xenoliths of Grt-peridotites
xenoliths of Sp-peridotites
dunites from ophiolites
harzburgites from ophiolites
chromitites from ophiolites

Figure 2a

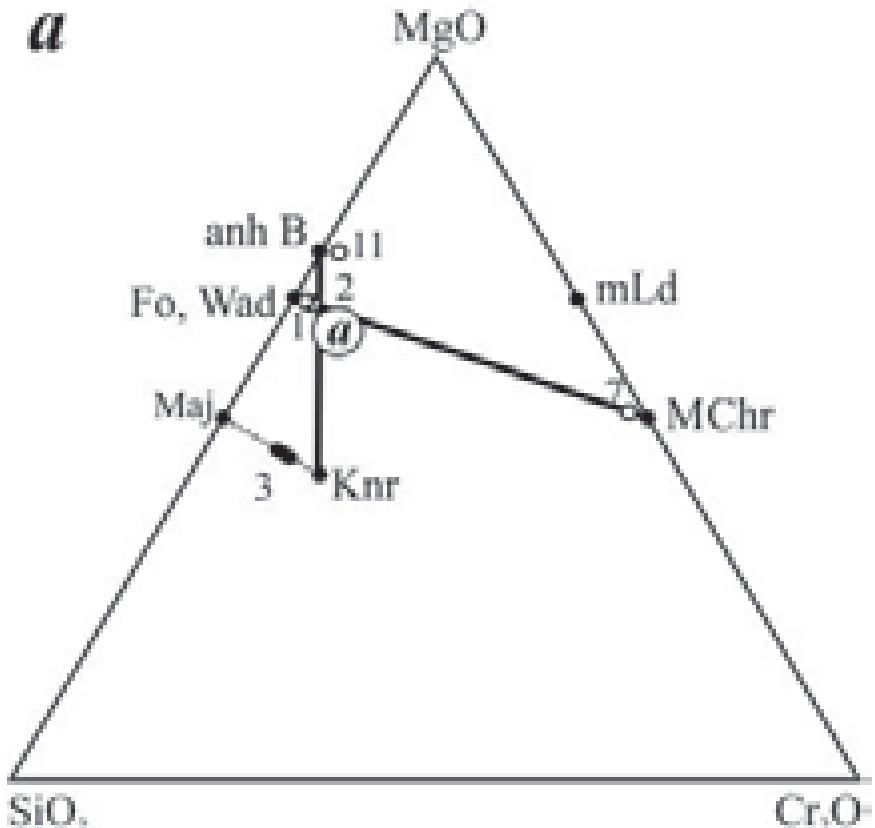

Figure 2b

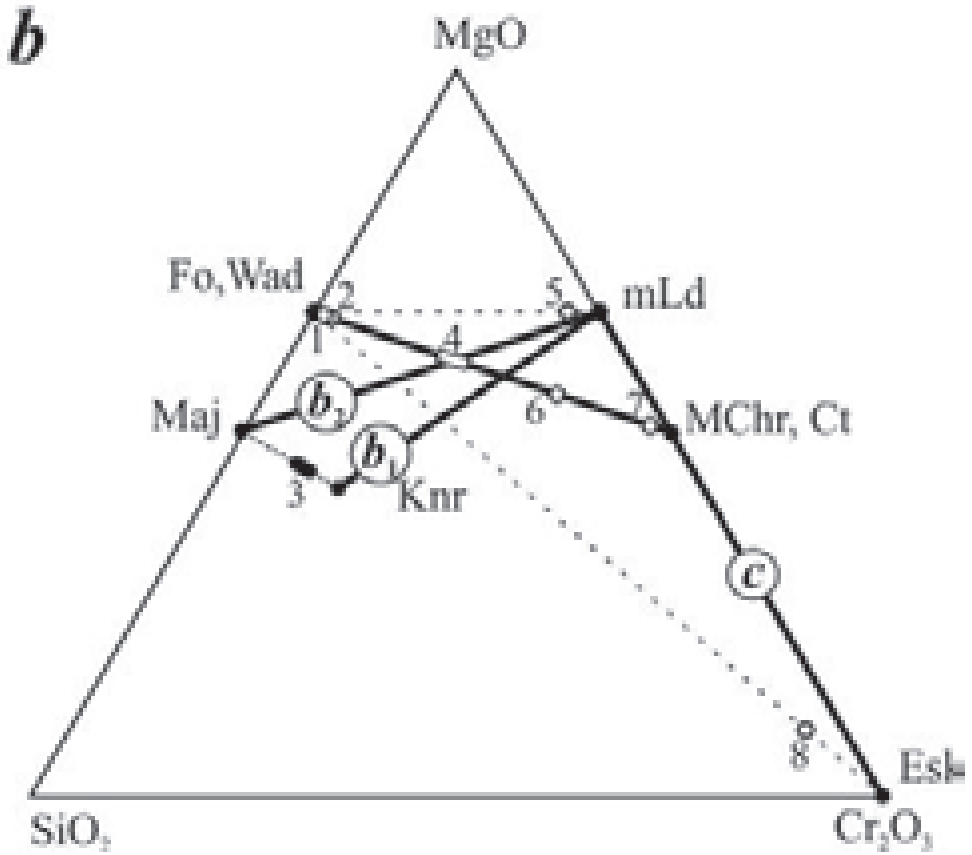

Figure 2c

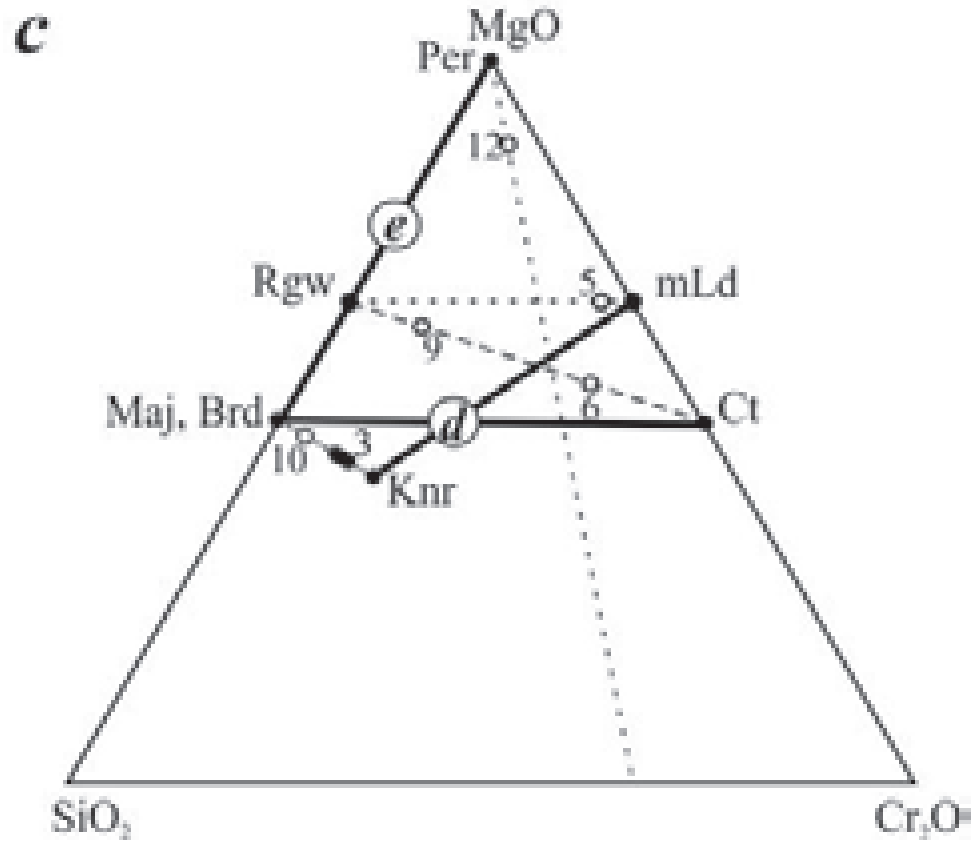

Figure 3

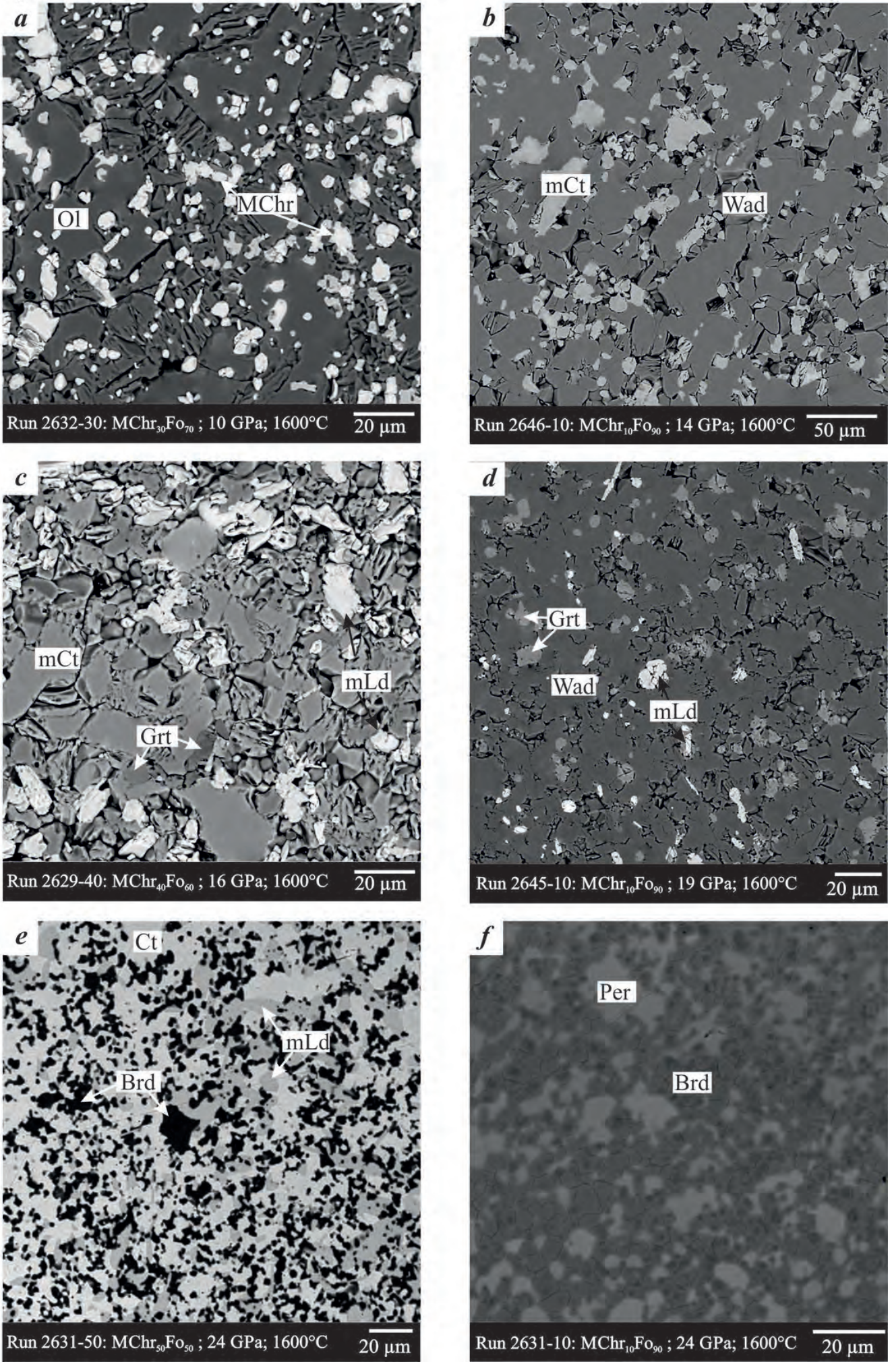
a
Ol
MChr
Run 2632-30: MChr30Fo70 ; 10 GPa; 1600°C
20 µm
b
mCt
Wad
Run 2646-10: MChr10Fo90 ; 14 GPa; 1600°C
50 µm
c
mCt
mLd
Grt
Run 2629-40: MChr40Fo60 ; 16 GPa; 1600°C
20 µm
d
Grt
Wad
mLd
Run 2645-10: MChr10Fo90 ; 19 GPa; 1600°C
20 µm
e
Ct
mLd
Brd
Run 2631-50: MChr50Fo50 ; 24 GPa; 1600°C
20 µm
f
Per
Brd
Run 2631-10: MChr10Fo90 ; 24 GPa; 1600°C
20 µm

Figure 4

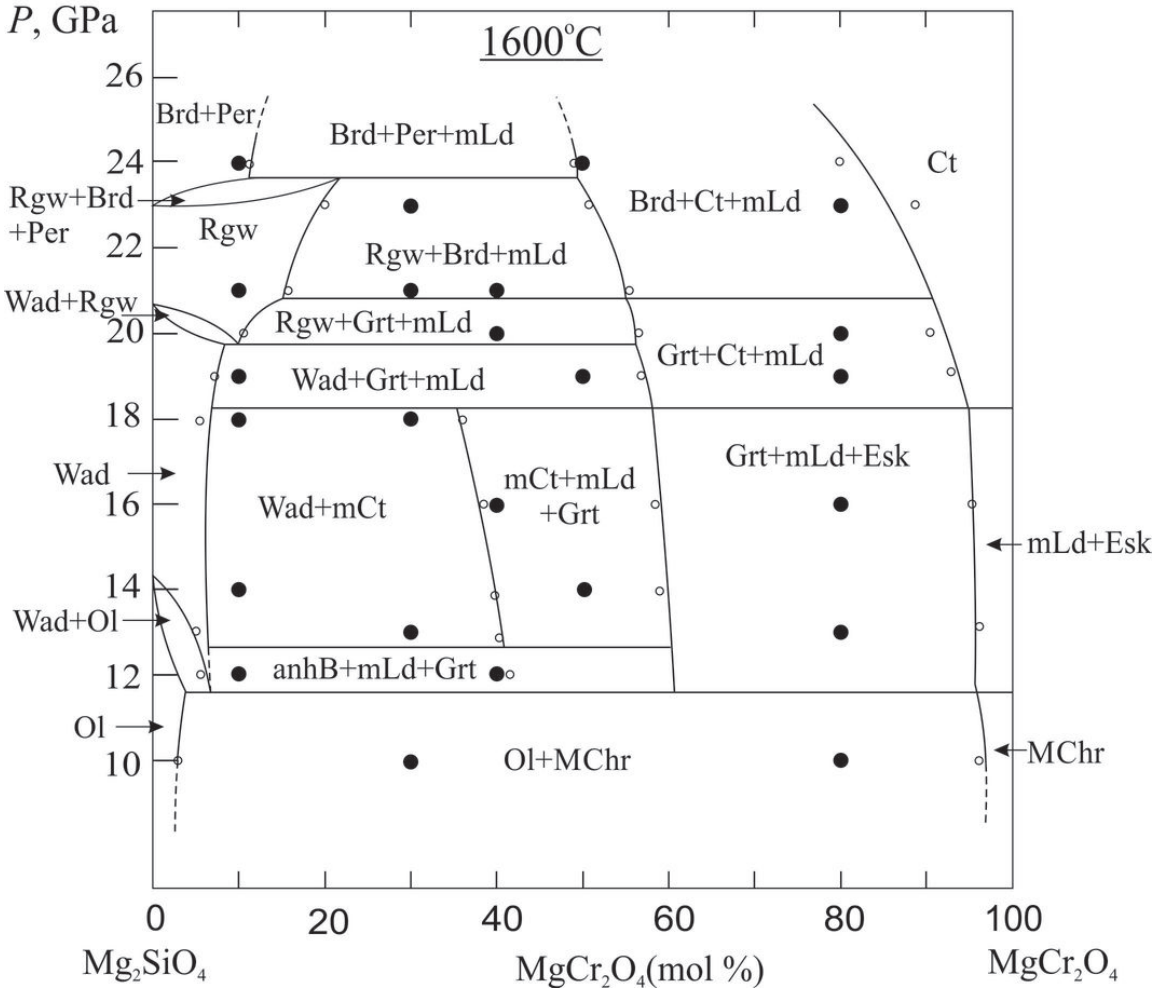
P, GPa
1600°C
26
24
22
20
18
16
14
12
10
Brd+Per
Brd+Per+mLd
Ct
Rgw+Brd
+Per
Rgw
Brd+Ct+mLd
Rgw+Brd+mLd
Wad+Rgw
Rgw+Grt+mLd
Grt+Ct+mLd
Wad+Grt+mLd
Grt+mLd+Esk
Wad
mCt+mLd
+Grt
Wad+mCt
mLd+Esk
Wad+Ol
anhB+mLd+Grt
Ol
Ol+MChr
MChr
0
20
40
60
80
100
Mg2SiO4
MgCr2O4(mol %)
MgCr2O4

Figure 5

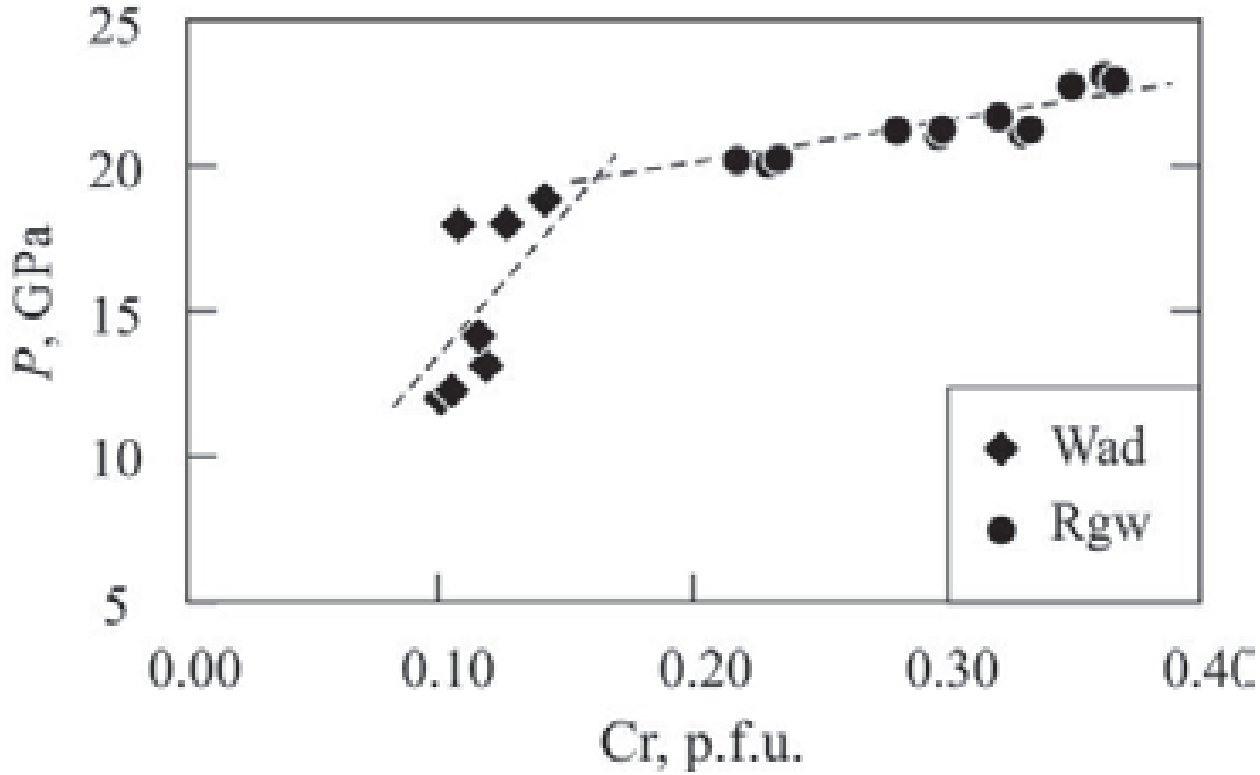

Figure 6

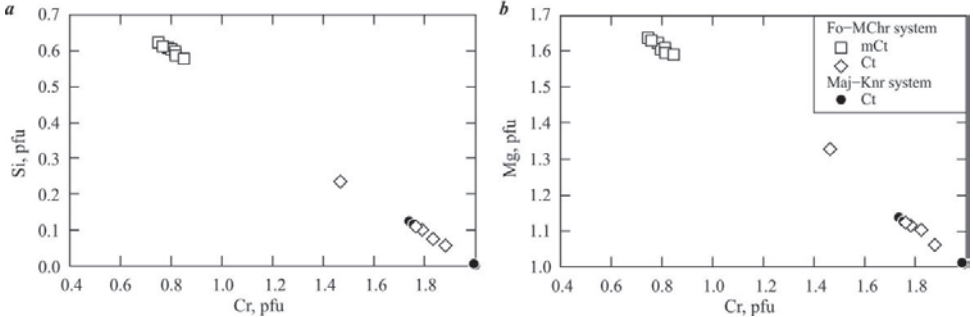
a
Si, pfu
Cr, pfu
b
Mg, pfu
Cr, pfu
Fo–MChr system
mCt
Ct
Maj–Knr system
Ct

Figure 7

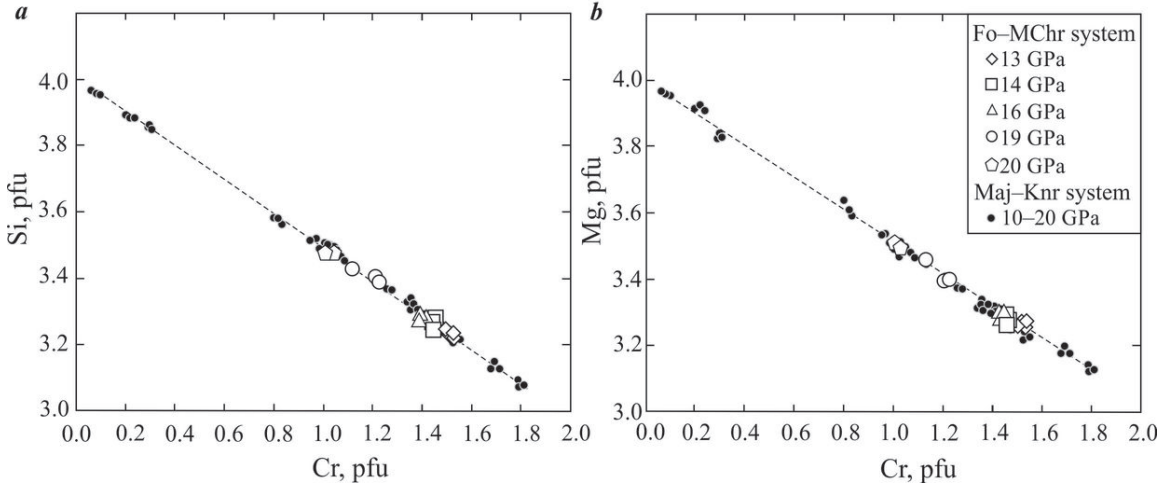
a
b
Si, pfu
Mg, pfu
Cr, pfu
Cr, pfu
4.0
3.8
3.6
3.4
3.2
3.0
0.0
0.2
0.4
0.6
0.8
1.0
1.2
1.4
1.6
1.8
2.0
Fo–MChr system
13 GPa
14 GPa
16 GPa
19 GPa
20 GPa
Maj–Knr system
10–20 GPa

Figure 8

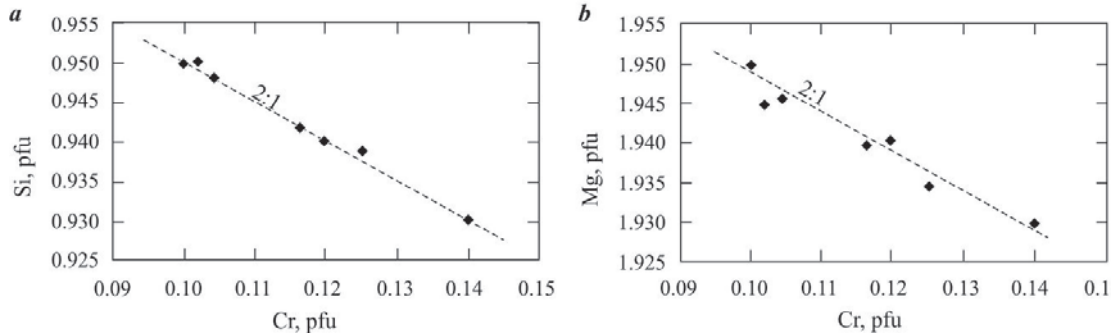
a
0.955
0.950
0.945
0.940
0.935
0.930
0.925
Si, pfu
2:1
0.09
0.10
0.11
0.12
0.13
0.14
0.15
Cr, pfu
b
1.955
1.950
1.945
1.940
1.935
1.930
1.925
Mg, pfu
2:1
0.09
0.10
0.11
0.12
0.13
0.14
0.15
Cr, pfu

Figure 9

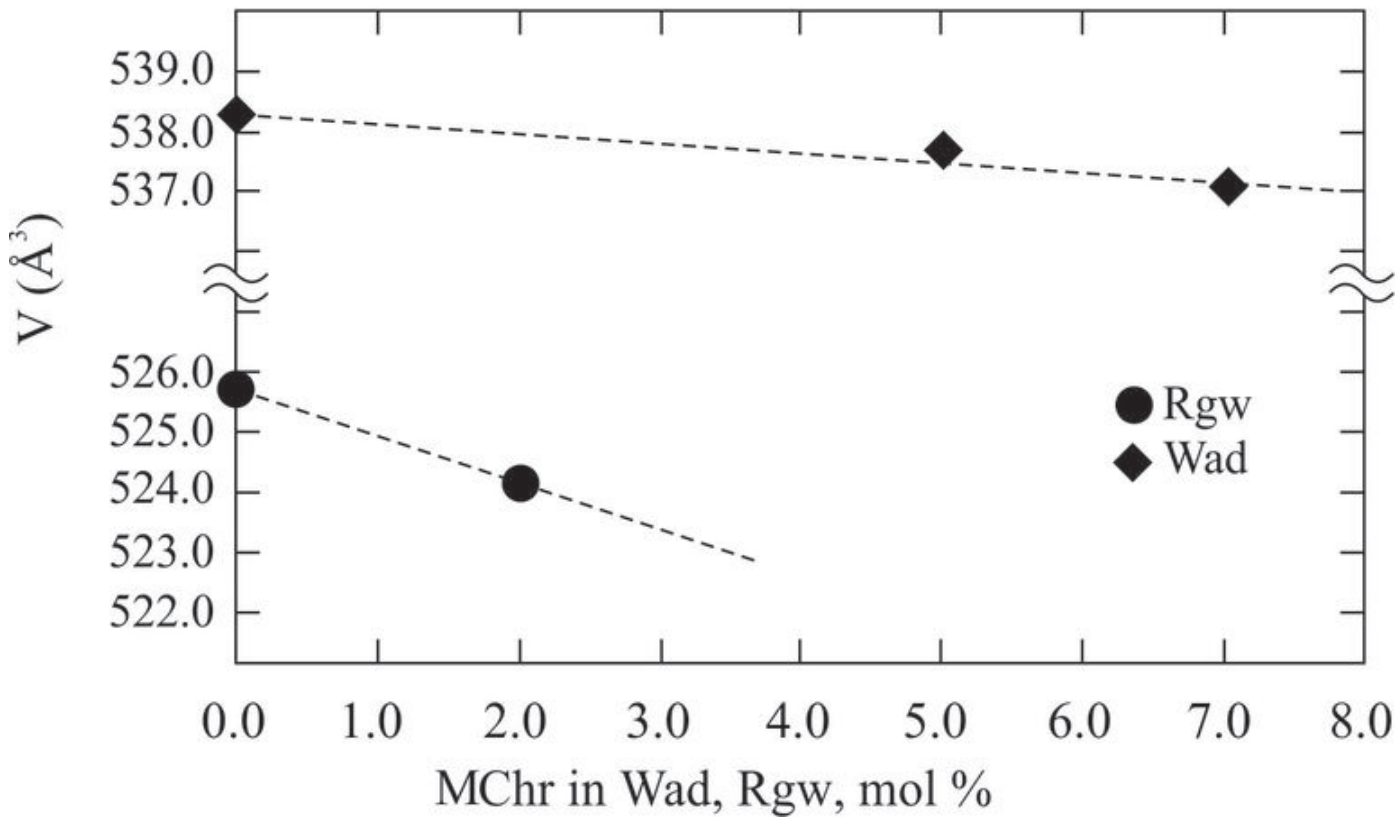
539.0
538.0
537.0
526.0
525.0
524.0
523.0
522.0
V (Å^3)
Rgw
Wad
0.0
1.0
2.0
3.0
4.0
5.0
6.0
7.0
8.0
MChr in Wad, Rgw, mol %

Figure 10

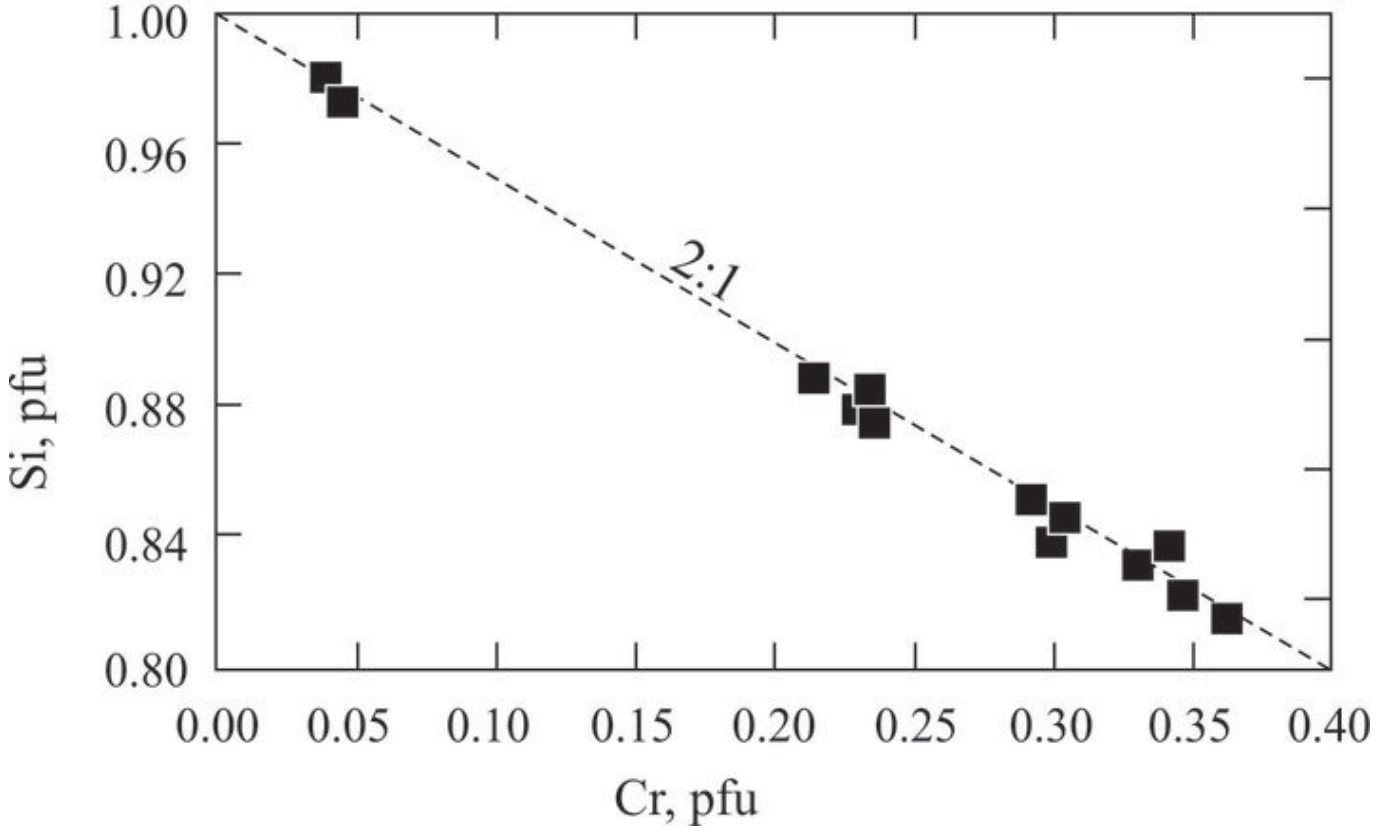
1.00
0.96
0.92
0.88
0.84
0.80
Si, pfu
2:1
0.00
0.05
0.10
0.15
0.20
0.25
0.30
0.35
0.40
Cr, pfu